Revealing the effect of stereocontrol on intermolecular interactions between abiotic, sequence-defined polyurethanes and a ligand

Maksymilian Szatko[a,b,#], Weronika Forysiak[a,c,#], Sara Kozub[a], Tadeusz Andruniów[b,*], Roza Szweda[a,d,*]

[a]M. Szatko, W. Forysiak, S. Kozub, Dr. R. Szweda
Łukasiewicz Research Network – PORT Polish Center for Technology Development
Stabłowicka 147, 54-066 Wrocław, Poland

[b]Prof. T. Andruniów, M. Szatko
Department of Chemistry, Wrocław University of Science and Technology
Wybrzeże Wyspiańskiego 27, 50-370 Wrocław, Poland
*E-mail: tadeusz.andruniow@pwr.edu.pl

[c]W. Forysiak
Faculty of Chemistry, University of Wrocław
F. Joliot-Curie 14, 50-383 Wrocław, Poland

[d]Dr. R. Szweda
Center for Advanced Technologies, Adam Mickiewicz University
Uniwersytetu Poznańskiego 8, 61-614 Poznań, Poland
*Email: roza.szweda@amu.edu.pl

#These authors contributed equally to this work

Keywords

stereocontrolled polymers, sequence-defined polymers, functional macromolecules, sensing, detection of bisphenol A, molecular dynamics, structure simulations

Abstract

The development of precision polymer synthesis has facilitated access to a diverse library of abiotic structures, wherein chiral monomers are positioned at specific locations within macromolecule chains. These structures are anticipated to exhibit folding characteristics similar to biotic macromolecules and possess comparable functionalities. However, the extensive sequence space and numerous variables make selecting a sequence with the desired function challenging. Therefore, revealing sequence-function dependencies and developing practical tools are necessary to analyze their conformation and molecular interactions. In this study, we investigate the effect of stereochemistry, which dictates the spatial location of backbone and pendant groups, on the interaction between sequence-defined oligourethanes and bisphenol A ligands. Various methods are explored to analyze the receptor-like properties of model oligomers and the ligand. The accuracy of molecular dynamics simulations and experimental techniques is assessed to uncover the impact of discrete changes in stereochemical arrangements on the structure of the resulting complexes and their binding strength. Detailed computational investigations providing atomistic details show that the formed complexes demonstrate significant structural diversity depending on the sequence of stereocenters, thus affecting the oligomer-ligand binding strength. Among the tested techniques, the fluorescence spectroscopy data, fitted to the Stern-Volmer equation, are consistently aligned with the calculations, thus validating the developed simulation methodology. The developed methodology opens a way to engineer the structure of sequence-defined oligomers with receptor-like functionality to explore their practical applications, e.g., as sensory materials.

1. Introduction

Sequence-defined polymers term was recently formulated to describe a macromolecule species whose length is discrete and the order of monomeric units within a chain is strictly specific.[1–4] Archetypical representatives of these chemical species are naturally occurring polymers, i.e. proteins and nucleic acids. Non-natural building blocks and backbones broaden the scope of macromolecular structures thanks to advancements in precision polymer synthesis.[5–8] Backbone structure may range from bioinspired peptoids[9,10], or polyphosphates[11] to novel chemical moieties, i. e., triazoles[12–14], urease[15], urethanes[16–19], ethers[20,21], esters[22,23], or π-conjugated oligomers.[24–27] Applying chiral monomers enables full control over the stereochemistry of macromolecules.[12,18,28–31] Consequently, primary structure control and stereochemistry are emerging as promising tools to induce functionalities in abiotic macromolecules.[32]

Discrete, abiotic macromolecules have already been proven to display functions like natural polymers. For instance, sequence-defined polymers are used as binary information carriers similar to DNA storing genetic code.[33–36] The encoded digital data can be revealed by mass spectrometry[37–39] or nanopore sequencing.[40] Interestingly, a relevant design of abiotic polymer structure enables for editing of encoded information by the light trigger.[41] Besides data storage, such macromolecules have been used in catalysis[42,43], drug delivery[44–48], sensing[27,49–51], selective binding[52,53], molecular transport[47,54], or as peptidomimetic foldamers.[55,56] The biological environment, where natural macromolecules perform sophisticated functions, is chiral. Therefore, the stereochemistry of macromolecules should be an essential parameter for their function. However, the effect of stereochemistry on polymer function has not been widely explored.

In general, the functionalities of biological macromolecules derive from their ability to arrange their chains spatially, attaining a three-dimensional structure. It is dictated by a sequence of

monomers characterized by various pendant substituents and stereochemistry. Stereocontrol opens up the possibility to influence the abiotic macromolecule interactions with the chiral, biological environment.[53,57,58] Stereospecificity, in combination with monomer sequence control, offers a wide library of abiotic structures to engineer functional macromolecules in a broad range of chemical and physical properties. However, very little is known about the sequence-structure-function relationship of abiotic macromolecules, particularly those built on non-amide backbones. Therefore, engineering selective functionalities into abiotic polymers remains beyond reach due to the enormous sequence space generating multiple variables that impede rational structure design until effective tools for characterizing their functionalities become available. The lack of a precise methodology impedes the characterization of their structural properties and the assessment of their functionality. While taking cues from related protocols developed in biosciences is possible, the intricate nature of studying nuanced properties, both structural and functional, often renders the direct transfer of these methods challenging.

Here, the impact of sequence stereospecificity on receptor-like functionalities of model oligourethanes towards the target molecule - bisphenol A (BPA) was investigated by computational and experimental methods. BPA and natural [3H]estradiol compete in the binding process to the estrogen receptors; therefore, it is an endocrine-disruptive substance and should be monitored in the environment.[59,60] The verification of molecular dynamic simulation outcomes by experimental techniques contributed to the development of a precise, computational tool for the characterization of receptor-like functionalities of non-natural, sequence-defined oligourethanes. The developed methodology opens a way to engineer the structure of sequence-defined oligomers with receptor-like functionality to explore their practical applications, e.g., as sensory materials.

2. Results and Discussion

Library of model oligourethanes with one (OU1-OU4, Fig. 1) or two mutations (OU5-OU7, Fig S1) of stereocenters were evaluated towards an ability to bind BPA ligand. Following the peptidomimetic nomenclature, studied molecules may be considered γ-peptide derivatives[61–63]. The resonance stabilization of the urethane bond tends to foster a planar conformation[64], which promotes the folding of those scaffolds. Therefore, we hypothesized that oligourethane scaffolds built from chiral monomers can attain a specific set of shapes in solution depending on the arrangement of stereochemically distinct monomers that affect their interactions with the ligand. Oligourethane sequences with methyl and benzyl pendant substituents are assumed to exhibit attractive interactions with the BPA (Fig. 2). BPA is a symmetrical molecule composed of two phenol rings connected via tetrahedral carbon with two methyl groups. Therefore, BPA is expected to form hydrogen bonds with urethane backbone groups and π-π stacking/van der Waals (vdW) interactions with oligomer side groups.

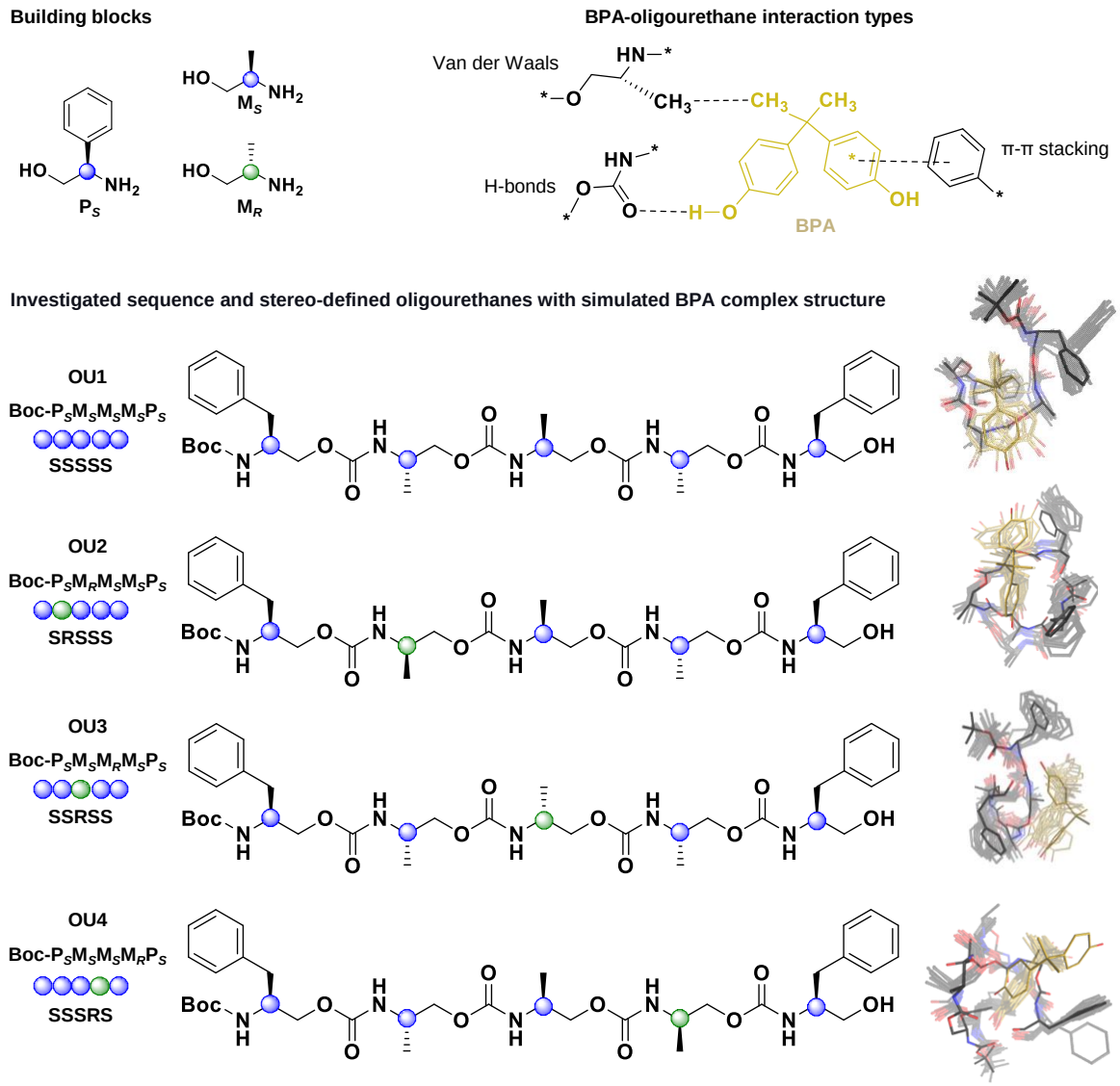

Figure 1. In this study, oligomers consist of aromatic (P_S) and aliphatic (M_S, M_R) monomers with a defined stereochemistry. Structures are designed to foster attractive interactions with BPA, encompassing H-bonds, Van der Waals, and π-π stacking forces. The depicted collection of discrete oligourethanes OU1-OU4 contains one mutation of one stereocenter in various positions. Structures of oligourethane-BPA complexes are received from the Multiple Simulated Annealing - Molecular Dynamics (MSA-MD). For clarity, all hydrogens have been hidden, and nitrogen and oxygen are represented by blue and red, respectively. BPA atoms are colored yellow.

2.1. Characterization of oligourethanes

Investigated stereocontrolled, discrete oligourethanes (OU1-OU7, Fig. S1) were synthesized according to the solution synthesis protocol using chiral monomers (P, M_S, M_R, Fig. 1) as described previously.[18] The structures of products were confirmed by size-exclusion chromatography (SEC) (Fig. S2-S8), LC-MS (Fig. S9-S15) and ^{1}H NMR (Fig. S16-S22) analyses. For all oligomers, SEC analyses yielded a single, narrow signal proving the uniform structure of oligomers. Overlapped GPC chromatograms show that each oligomer is characterized by a specific retention time that indicates the stereochemistry-dependent hydrodynamic volume of oligomer chains (Fig. S8B). In LC-MS chromatograms, we observed one peak corresponding to oligomer molar mass. As expected, for all studied diastereoisomers we observed three main signals at m/z 632.33, 732.38 and 754.36 corresponding to ions $[M\text{-}Boc+H]^+$, $[M+H]^+$ and $[M+Na]^+$, respectively.

^{1}H NMR analyses revealed structural differences between oligomers depending on the sequence of stereocenters indicating various spatial conformation preferences (Figure 2A-2F, S16-S22). In the spectra, we distinguished six signal regions which are coming from aromatic protons at 7.0-7.5 ppm (I), urethane N-H at 4.6-6.75 ppm (II), backbone protons at 3.5-4.5 ppm (III), -CH_2- from benzyl side chain at 2.5-3.0 ppm (IV), methyl side chains at 1-1.2 ppm (V) and Boc protons at 1.40 ppm (Boc), as presented in Fig. 2A. At room temperature, protons from backbone and methyl side chains occur as broaden multiplets with sequence-specific patterns (Fig, 2B-F) defined by a diverse spatial arrangement of chiral building blocks. The sequence conformation stability can be assessed based on the Boc ^{1}H NMR signal as an internal probe (experiment at 240K), which delivers information about the homogeneity of the Boc neighborhood reflected in a signal splitting (Fig. 2F).

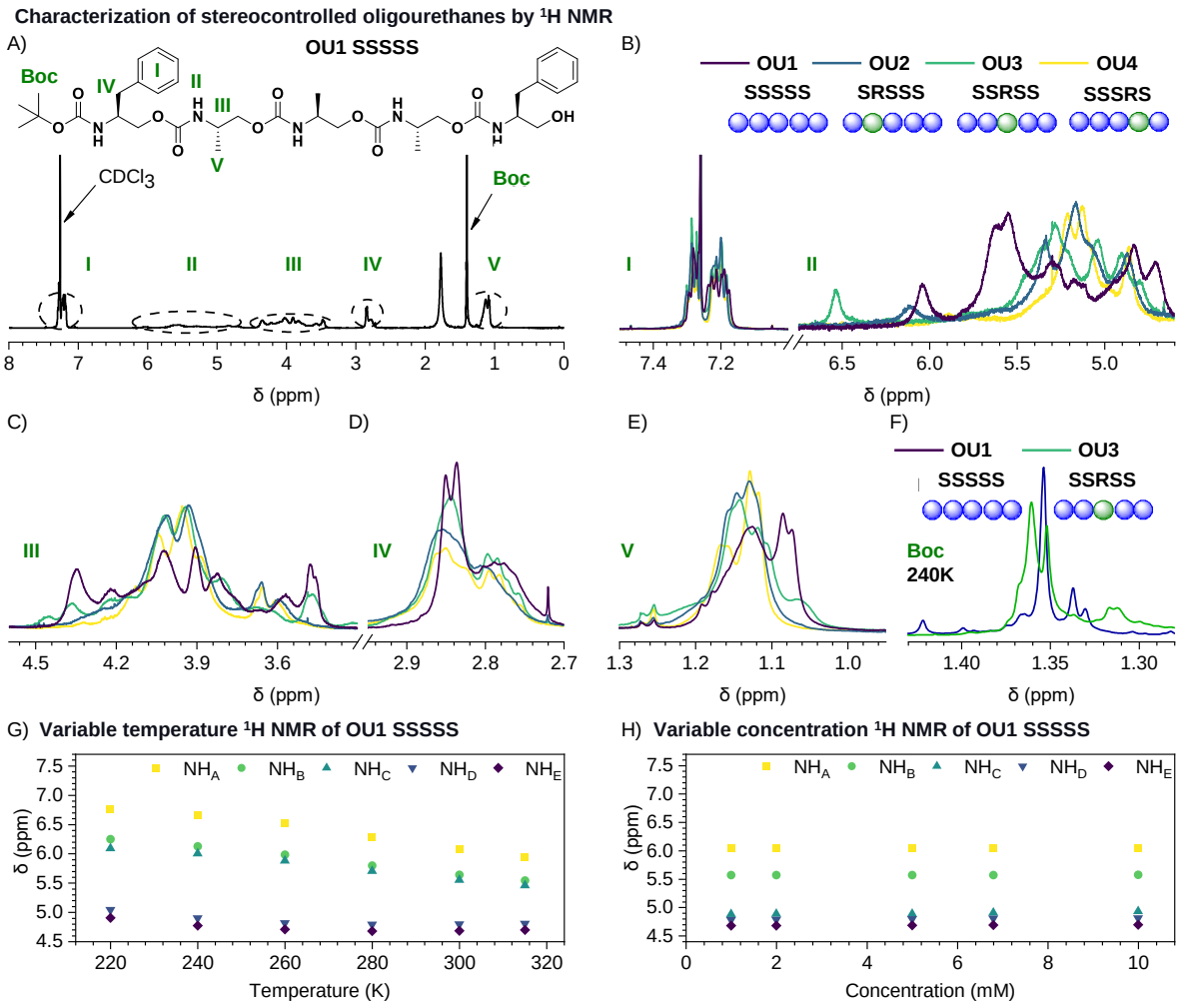

Figure 2. ^{1}H NMR characterization of stereocontrolled oligourethanes revealed differences between oligomers depending on the sequence of stereocenters. (A) Representative ^{1}H NMR spectrum of OU1 SSSSS. Upon zooming individual regions, I (H-Ar, B), II (H-N, B), III (backbone protons, C), IV (-CH_2-Ar, D), V (-CH_3, E) spectrum shape dependence on stereochemical sequence for OU1-OU4 with one stereocenters mutation becomes apparent. Sequence-specific splitting of the Boc signal is noticed, indicating the distinct conformational preferences of studied oligomers (F). Variable temperature experiments (6.8 mM) indicate the formation of intramolecular hydrogen bonds (G). A notable chemical shift in N-H protons upon temperature decrease is evident, where no change occurs during the variable concentration experiment in the range of 1-10 mM (H), confirming that the hydrogen bonds come from the single-chain folding.

The decrease in temperature improves the resolution of the signals causing the stabilization of conformation and formation of energetically favored structures (representative ^{1}H NMR variable temperature spectra for OU1 and OU2 see Fig. S23-S24). The decreased temperature has diminished the exchange rate between conformations of oligourethanes, highlighting the uniqueness of shapes for each stereosequence. Moreover, cooling causes significant alterations of urethane N-H proton chemical shifts, indicating the presence of intramolecular hydrogen bonds (Fig. 2G, S24, S26).[65,66] The possibility of intermolecular hydrogen bond formation due to the aggregation of macromolecules was disproved through variable concentration ^{1}H NMR experiments in the range of 1-10 mM. Upon changes in concentration, values of N-H chemical shifts remain constant. Therefore, obtained data suggests that within the studied concentration range, we observe intramolecular hydrogen bonds from single-chain folding (Fig. 2E, S25-S26). All investigated oligomers display conformational preferences, and their conformations depend on the sequence of stereocenters; therefore, each oligomer represents a unique set of shapes in the solution. Further, we examined how stereocenter mutations affect the formation of oligourethane-BPA complexes to assess the impact of stereochemistry on their receptor-like function.

2.2. Studies of the oligourethane-BPA interactions by Molecular Dynamics

Molecular dynamic simulation studies revealed details on oligourethane-BPA structures. Extensive multiple simulated annealing molecular dynamics (MSA-MD) computational protocols followed by clustering were employed to characterize the conformational space of investigated oligourethane-BPA complexes solvated in the implicit chloroform. Simulated annealing was performed for 150 ps by heating from 298K to 500K, equilibrating, and finally reducing the temperature to 0K. These calculations were repeated 300 times with randomly generated velocities using the Maxwell-Boltzmann distribution. The applied procedure generates a set of random local minima which were the starting configurations for 10 ns MD

simulations at 298K. In all simulations Amber14SB[67] force field parameters were employed for oligourethane-BPA complexes. More technical details on simulation parameters are provided in the Supporting Information (Section 4.2). Structures derived from the trajectories of the oligourethane-BPA complex were organized into clusters based on the structural resemblance, corresponding to a specific conformation. Out of 42 866 structures representing the whole ensemble, the 5 most populated clusters were selected and analyzed from a structural standpoint for each oligomer OU1-OU7 (Fig. S27). Depicted 5 clusters represent, on average, 60% of the ensemble, whereas a dominant cluster characterizes ca. 20% of all conformations. Representative cluster distributions for oligourethane-BPA complexes with one stereocenter mutation are shown in Fig. 3. Simulated three-dimensional structures of oligomer-BPA complexes for dominant clusters are visualized in Fig. 1. It is seen that the structure of the complexes solely depends on the stereoconfiguration of the oligomer. The 3D structure of oligourethane with associated BPA varies among the clusters, inferring that the complexes exhibit conformational flexibility. Oligomer chains adopt diverse shapes, to which BPA binds, generating a range of complex conformations that undergo an interchange.

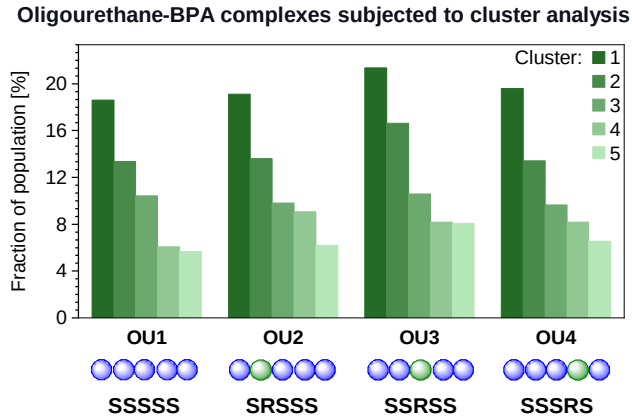

Figure 3. The representative cluster distributions for oligourethanes with a single stereocenter mutation, OU1-OU4, complexed with the BPA. The cluster analysis was performed based on the structural similarity of BPA-oligomer complexes.

Backbone torsional angles are used to analyze conformations of oligourethane-BPA complexes identifying a sequence-shape dependency. Structural biology uses the Ramachandran method to graphically analyze the rotation of peptide bonds in the protein chain. Due to steric hindrances and hydrogen bonds, allowed and disallowed torsional angle regions are created, impeding rotations. Their analysis enables one to assess the shape and stability of the three-dimensional structure of the macromolecule. Since urethanes can be considered peptide bond relative, the Ramachandran plot methodology was modified to investigate abiotic oligourethanes. We used nomenclature, which refers to the initially developed for peptide bond analysis and defined ψ (C–O), ω (C–N), and φ (N–C_γ), torsions. In the case of urethanes, the backbone is extended by two rotatable bonds, and that obliges us to also introduce ξ (C_γ–C_β) and χ (C_β–O) torsions (Fig. 4A). Yet not all torsions are valid for the analysis, i.e., C–O and C–N bonds, in urethane group, are affected by electron resonance, thus making ψ and ω torsions immobile and making urethane groups stiff and planar. When remaining rotations φ, ξ, and χ are analyzed separately, distinct torsional preferences within these systems are unveiled.

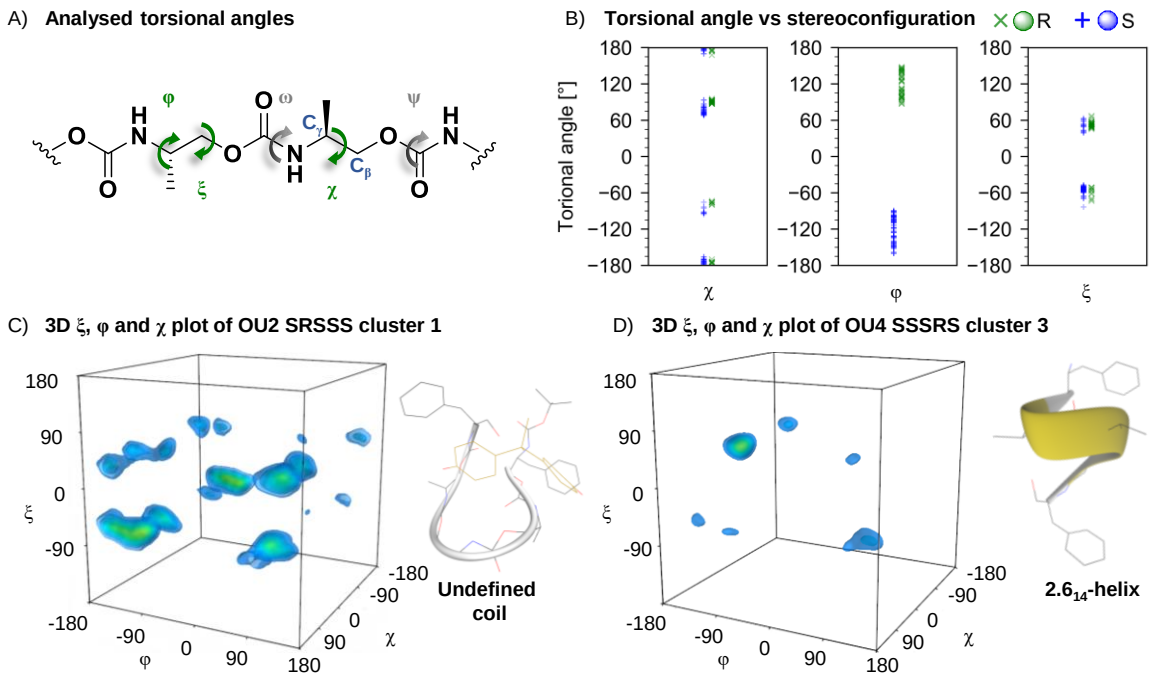

Figure 4. The shapes of oligourethane-BPA complexes can be depicted through graphical analysis of their torsional angles φ, ξ, and χ. (A) The fragment of a urethane chain shows the projected bond rotations, defining individual torsional angles. (B) The most probable φ, ξ, and χ angle values plotted with respect to the stereochemistry visualize apparent torsion preferences. The analysis involved deriving the highest probability angle values for each monomer within every cluster while considering their stereochemistry. By assessing all mutual angle dependencies via the 3D torsional plot, an example of angle distributions for conformations respective to the undefined coil (C) or right-handed helix structure (D) is revealed and depicted in NewCartoon style.

We observed that φ dihedral value is dependent on the stereochemistry of the Cγ atom. The data shows its values are distributed around 120° or -120°, depending solely on the stereochemistry of the introduced monomer. The φ torsion value is < 0 if the monomeric unit is of S configuration, and otherwise, φ assumes > 0 values if the configuration is R (Fig. 4B). Whereas no effect of stereoconfiguration is observed for two other torsions ξ and χ. The ξ torsion values oscillate around 60° or -60° disregarding the stereochemistry. The third torsion χ assumes 4 possible values in proximity to -180, -70°, 70° or 180°, similarly, no stereochemical effect has been identified.

Analyzing three angles collectively offers insights into their mutual presence and enables to extract the structural information. Every set of clusters is composed of a unique distribution of φ, ξ and χ angles, which reflects the multitude of chain arrangements and possible interaction sites to which BPA binds. Most of the torsional plots for oligourethane-BPA complexes are characterized by multiple, widely distributed values, which reflect undefined coil arrangements, far from helix and sheet characteristics for biomacromolecules (e.g., OU2 SRSSS - cluster 1, Fig. 4C, for other examples see Fig. S30 and S32). Among analyzed clusters, we found examples of structural regularity indicating the presence of helical structure (OU4 SSSRS

cluster 3 and OU6 SRSRS cluster 5 depicted in Figures S29 and S31, respectively). For example, cluster 3 of OU4 SSSRS folds into a misshaped right-handed helix, which occurs 9.6% of the simulated time. The helix structure depends on interactions between monomers in the chain and BPA ligand, which may act as a structure-disrupting agent, thus influencing the stability and regularity of the formed complex. The clusters represent groups of similar complex conformations, not isolated oligomers, hence, a lack of structural regularity is expected.

To look into the structural peculiarities of the complex, we studied the formed hydrogen bonding network. An analysis of intra- and intermolecular hydrogen bonds representing electrostatic interactions in the oligourethane-BPA complexes is presented in Fig. 5. The ensemble average analysis provided a general perspective on data analysis (Fig. 5A). We see that in complex formation, one hydrogen bond is formed intramolecularly by oligomer, and one is used to couple with BPA. The input of H-bonds differs between oligomers. Specifically, when the chirality mutation from S to R occurs at the third position in the sequence, we observe an increase in the contribution of both inter- and intramolecular hydrogen bonds. The analysis of individual clusters (Fig. 5B) shows that in most cases, we observe the inversely proportional tendency of inter/intra hydrogen bond formation. The clusters (OU1-OU3) with the highest input of intramolecular hydrogen bonds exhibit the lowest involvement of intermolecular hydrogen bonds. The data suggest that BPA may compete for the donors and acceptors of hydrogen bonds of oligourethane. Interestingly, the exception is the OU4 sequence, for which the formation of a unique helical complex was observed. The analyzed helix structure of the SSSRS cluster displays an average of 1.29 intramolecular hydrogen bonds, just slightly higher than the overall average across the entire SSSRS complex ensemble – 1.01 hydrogen bonds, indicating that structure regularity might not correlate with the number of hydrogen bonds in those systems.

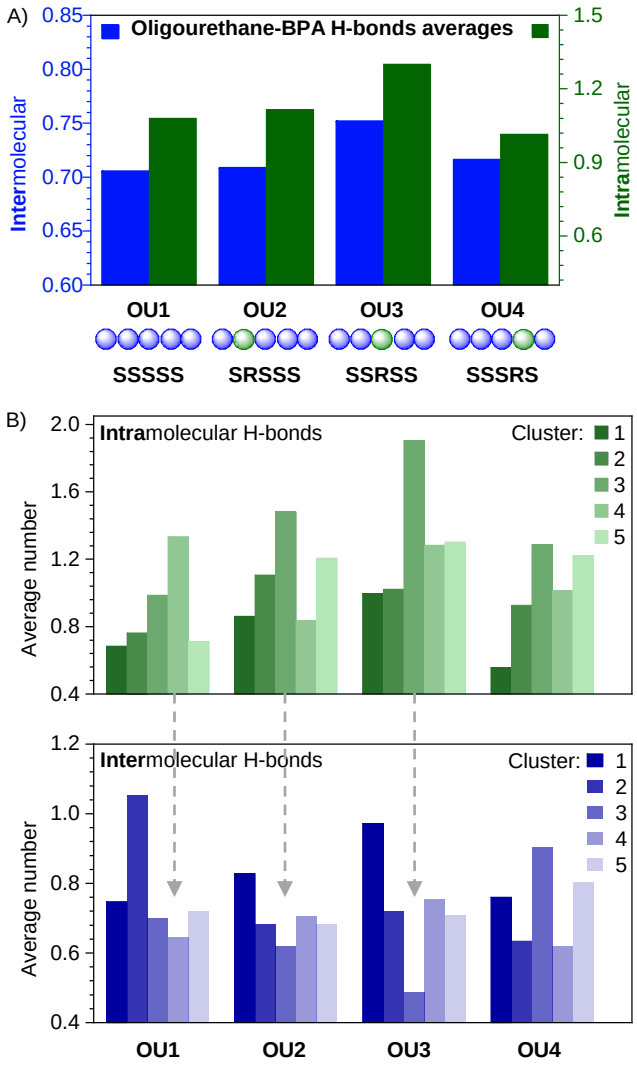

Figure 5. The ensemble average of both intra- and intermolecular hydrogen bonds reveals stereochemistry-dependent characteristics. (A) An inversion of the stereocenter at the third position in the oligomer chain results in an increased count of hydrogen bonds of both types (analysis of the whole ensemble). (B) The analysis of hydrogen bond number averages by individual clusters suggests an inverse tendency of inter-intra hydrogen bond formation.

The receptor-like functionality of the studied oligourethanes (OU1-OU7) was demonstrated through variations in Gibbs binding energy values (ΔG_{bind}) calculated for oligourethane-BPA complexes. We found that ΔG_{bind} varies with the stereochemistry of the oligomer as shown by the Molecular Mechanics – Generalized Born Surface Area (MM-GBSA) calculations (Fig. 6).[68] The details of the calculations are provided in the Supporting

Information. To visualize the general influence of mutations of stereocenters on BPA binding, the average ΔG_{bind} for the whole ensemble has been calculated (Fig. 6A). For all investigated complexes its values range from -7.70 kcal/mol to -8.70 kcal/mol between oligomers (Table S4), and each oligourethane-BPA system is characterized by a unique set of binding force magnitudes (Fig. S34A). The data clearly shows that the stereoconfiguration modulates the intermolecular binding function that relates to the diversity of attained structures. The stereochemical center manipulation has the most prominent effect if the middle monomer is mutated to the opposite configuration (OU3 SSRSS).

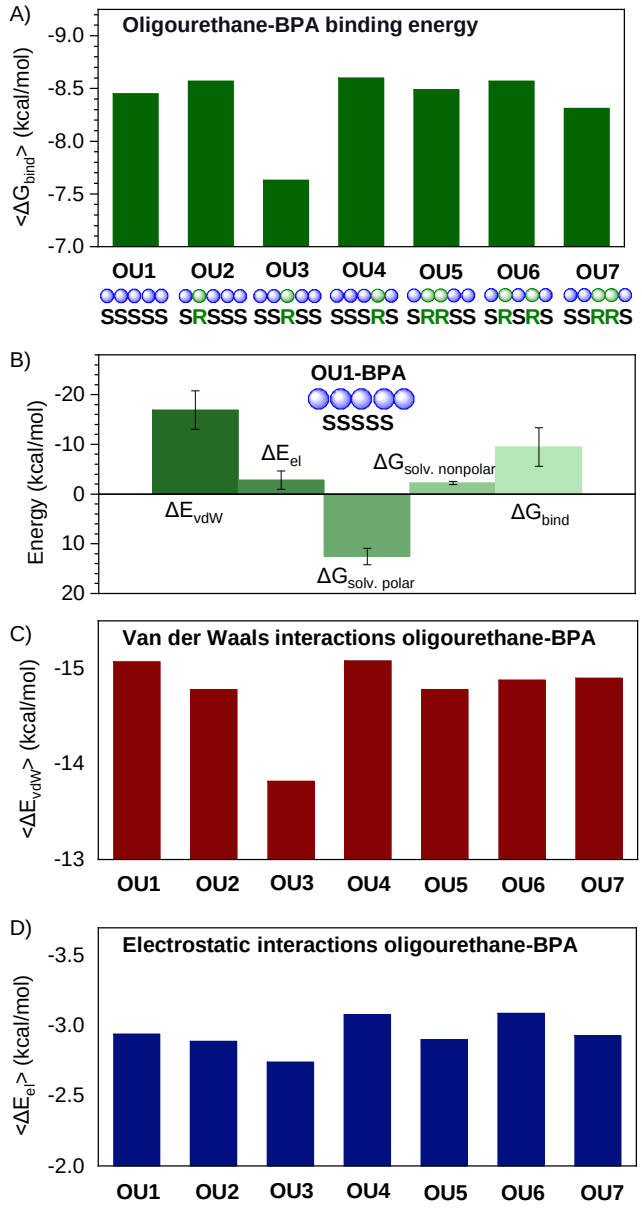

Figure 6. The analysis of receptor-like functionality of stereocontrolled oligourethanes by Gibbs binding energy calculations. The average ΔG_{bind} values show a substantial variance, indicating that each oligomer engages the ligand with characteristic strength (A). When ΔG_{bind} for the OU1-BPA complex is decomposed into its energy components (B), a main contribution of dispersive forces ΔE_{vdW} to the binding process becomes evident. The bars on the chart indicate the statistical distribution of energy values for the whole ensemble. C) The ΔE_{vdW} values for each oligomer-BPA complex. D) Contribution of electrostatic interactions ΔE_{el} to the oligourethane-BPA binding.

Through decomposition analysis of ΔG_{bind} energies (depicted in Fig. 6B), we gain insights into the nature of interactions between the oligomer and ligand. Two major components of ΔG_{bind} are van der Waals energy (ΔE_{vdW}) and electrostatic energy (ΔE_{el}) representing two molecular mechanics non-bonding terms describing non-covalent interactions. Other elements of ΔG_{bind} value comprise interactions between solute and continuous solvent divided into polar ($\Delta G_{solv.\ polar}$) and non-polar ($\Delta G_{solv.\ nonpolar}$), which constitute free energy of solvation ($\Delta G_{solv.}$) dominated by the polar component representing repellent force (Fig. S34B, C). For all studied oligomers, the total effect of solvation energy gives a positive value, which depends on the complex shape. Thus, the data indicate that the solvent-accessible surface area and available polar interactions relate to the stereochemistry of oligourethane. The dominant contribution to ΔG_{bind} is vdW interaction indicating that dispersive forces are the major forces responsible for complex formation. The mutation of stereocenters leads to the changes of ΔE_{vdW} above 1.23 kcal/mol (Fig. 6C). In the case of electrostatic interactions which involve hydrogen bonds, the variations in the ΔE_{el} value with stereochemistry are minor, differences are below 0.3 kcal/mol (Fig. 6D). Interestingly, the highest ΔE_{el} values are observed in the case of complexes (OU4 and OU6) that can attain the helical conformation.

2.3. Experimental analysis of oligomer-BPA interactions

Establishing a relevant protocol adjusted to the studied system is critical to getting reliable information about the interaction between molecules. Numerous experimental methods are applied to analyze molecular interactions, which are mostly validated for biological systems.[69,70] We evaluated NMR,[71] circular dichroism[72,73], and fluorescence spectroscopy[74–76] techniques to study oligourethane-BPA interactions.

Formation of the complex causes changes in the chemical environments of protons belonging to the binding molecules that can be followed by NMR. ^{1}H NMR analyses of oligourethane-BPA complexes (oligomer:BPA, 1:1 molar ratio) revealed alterations in spectra compared to characteristics of individual compounds (Fig. 7A, S36-S42). We observe changes in the shape of signals coming from N-H protons meaning that BPA is disturbing the oligomer hydrogen bond net. The most noticeable deviations in the spectra appear in the aromatic region, where we observe a clear shift of signals attributed to aromatic protons of BPA. This characteristic shift of about 0.01 ppm is visible for all studied oligomers OU1-OU7, suggesting interactions between both molecules (Table S5). To confirm the formation of the complex we performed a 2D NOESY experiment for a representative OU5-BPA system. The analysis revealed cross-peaks between the aromatic signal of BPA and oligomer phenyl moiety (Fig. S35). Relatively small and irregular changes of ^{1}H NMR spectra, without a clear tendency, observed for oligomers upon BPA titration reflect the structural dynamics of complexes and the diversity of ligand binding sites, as presented by cluster analyses.[77] The chemical shifts of NMR signals are very structure-dependent, hence, studies of dynamic systems forming various complexes do not provide representative data of the whole ensemble, yet the obtained data confirm interactions between both molecules.

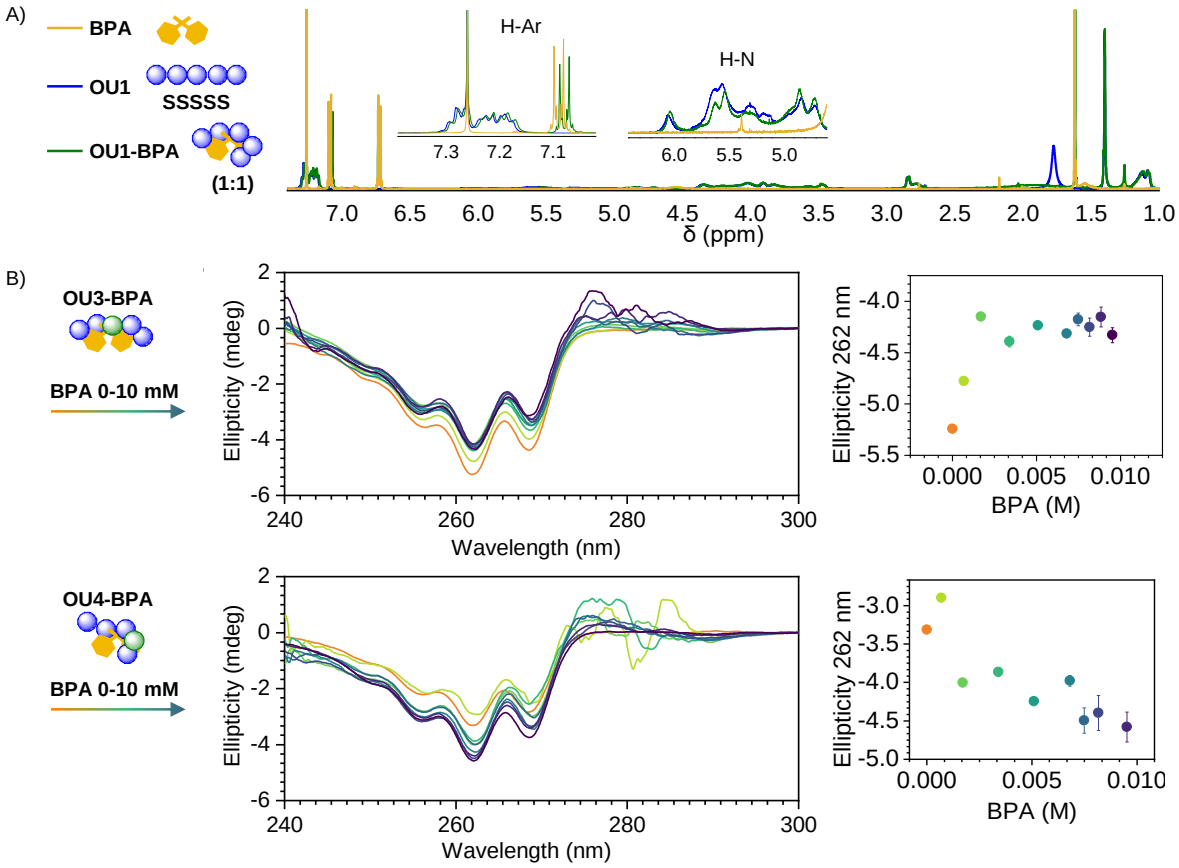

Figure 7. A) The superimposed ^{1}H NMR spectrum shows that the presence of BPA caused alteration of the signals. The greatest changes are visible in the range of amine and aromatic protons. B) Complex formation is observed via CD titration measurements. As the concentration of the BPA increased, an increase in the CD signal intensity was noted for OU3 SSRSS (top), signifying the emergence of the complex that impacts the spatial arrangement of the oligomer. On the contrary, a decrease of the CD signal was observed upon titration of BPA in the case of OU4-BPA SSSRS (bottom).

The chiral configuration of oligourethanes is an attribute that allows to investigate interactions between oligomers and BPA using circular dichroism spectroscopy. Oligourethanes built from aromatic chiral phenylalaninol monomers (P) show characteristic CD signals in the range 240-280 nm (Fig.S43-S49), therefore it may act as an excellent probe to follow structural changes of complexes as BPA is a CD silent ligand. Consequently, CD results demonstrate various interactions occurring between oligomer and BPA depending on stereochemical arrangements.

Increasing concentration of BPA ligand leads to a significant change in the CD signal intensity for all oligomers (Fig. 7B, S43-S49). All spectra apart from OU4-BPA SSSRS show an increase in CD signal amplitude. Remarkably, OU4 is a unique sequence where helical conformation has been found by molecular dynamics calculations. A change in the signal intensity indicates the formation of the complexes, affecting the three-dimensional structure of oligomers, which may be a consequence of adjustments in the skeletal conformation of oligomers to the ligand molecule. However, no typical titration trend matches the obtained CD intensity curves, apart from the SSRSS oligomer (Fig. 7B). Similar to NMR, CD spectroscopy is a technique revealing structural details of formed pairs, which demonstrates occurring interactions, yet unsuitable for representing a structurally diverse ensemble.

Investigated oligourethanes composed of P monomers with a benzylic substituent exhibit fluorescent properties, similar to phenylalanine-containing peptides, therefore, interactions with BPA can be followed by emission measurements.[78] Interactions between molecules often lead to alterations in the intensity, shape, or position of the receptor fluorescence signal, hence, fluorescence is employed as a tool to investigate molecule binding through the measurement of its quenching [79], enhancement[80], anisotropy[81] or shift[82] depending on the system. Oligourethanes are characterized by excitation and emission at the UV range with maxima at λ_{Ex}=260 nm and λ_{Em}=310 nm, while BPA exhibits weak activity within the specified wavelength range (Fig. S50). For all studied oligomers, BPA titration leads to significant quenching of fluorescence signal (Fig. 8A, S51-S57). The intensity changes were fitted to the Stern–Volmer equation to determine dissociation constant (K_d) values for all investigated systems (Fig. 8B).[83] Those values were inversed to obtain association constants (K_a), which were used as a representative parameter to describe the receptor-like functionality of oligourethane towards BPA and compared with theoretical ΔG_{bind} values derived from molecular dynamics (Fig. 8C).

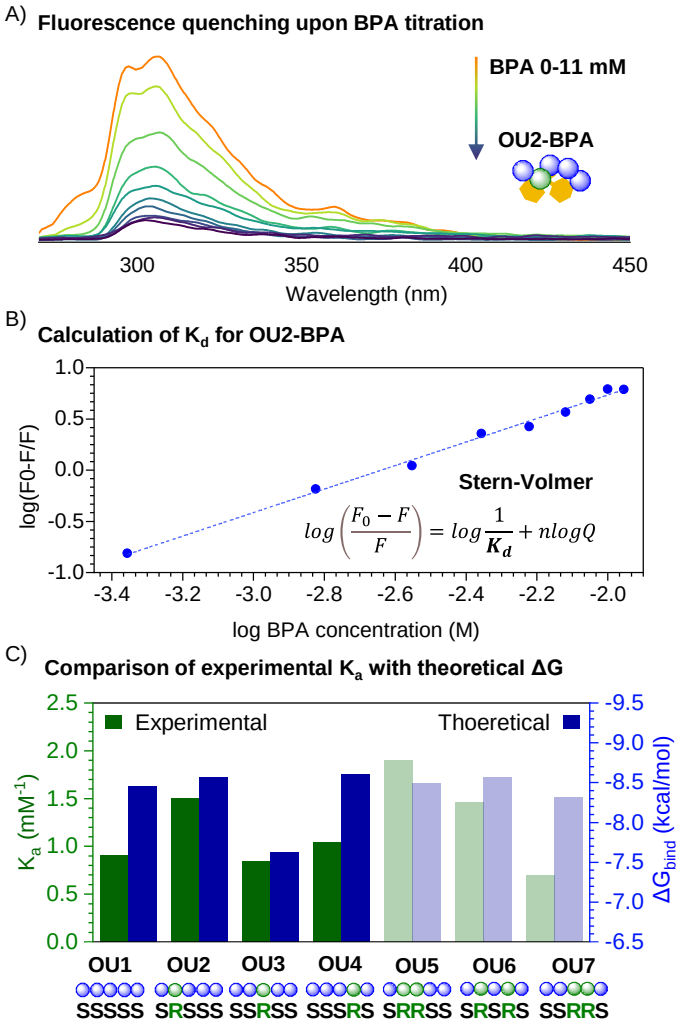

Figure 8. A) Fluorescence spectra of OU2 (68 μM) recorded in chloroform (orange). BPA titration (0-11 mM) causes quenching of oligourethane fluorescence. (B) Fluorescence quenching was used to calculate dissociation constant (K_d) values based on the Stern-Volmer equation, where F – the measured fluorescence, F_0 - fluorescence of oligourethane solution before BPA is added, and Q - quencher (BPA) concentration. C) Both experiment-derived K_a (K_a=1/K_d) and the theoretically calculated ΔG_{bind} demonstrate a compatible value variation depending on the sequence of stereocenters.

An alteration of the sequence of stereocenters influences K_a values, leading to a subsequent decrease in Gibbs free binding energy. Comparing the theoretical and experimental data across the entire library of oligourethane-BPA complexes reveals a consistent trend of changing

parameters that describe the receptor-like functionality of oligomers. Computational studies show an approximate 70% success rate in trend predictions. Notably, some oligomers displayed a significant decrease in K_a values with respect to ΔG_{bind}, indicating reduced stability of formed oligourethane-BPA complexes. However, discrepancies may relate to the mechanism of a quenching phenomenon that is not considered in calculations but can influence experimentally determined K_a. Nevertheless, both methods indicate which oligomer is characterized by the most promising receptor-like features (OU5) and appoints the least efficient sequence (OU3). The OU5 shows the most potent interaction with BPA among all studied systems, as indicated by experimental and theoretical approaches. At the computational level, OU5 is in the top 4 oligomers with the highest binding energy values. Differences between them are minor, e.g., a bit diverse value of ΔG_{bind} than for OU5 are revealed by OU2 (0.14 kcal/mol), OU4 (0.20 kcal/mol), and OU6 (0.04 kcal/mol). We did not notice a connection between the ability of oligomers to form a secondary helical structure (OU4 and OU6) and its effectiveness in BPA binding. A high number of hydrogen bonds does not guarantee strong binding, as could be expected. OU3, which forms the most hydrogen bonds (Fig. 5) is characterized as the weakest receptor (Fig. 8C). This observation highlights the leading role of hydrophobic interactions. The presented data emphasizes the importance of sequence programming through stereoconformation changes, which directly affects the spatial arrangement of the complex and the strength of binding with the ligand. The developed computational methodology enables the screening of abiotic oligomers and, in silico, identifies abiotic oligomers characterized by binding function toward chosen ligands, revealing stereochemistry effects.

3. Conclusions

The structural properties of sequence-defined oligourethanes hold a great potential to form nuanced shapes, which can be controlled by a rational design. Engineering non-natural

macromolecule functionalities demands effective tools to study their conformation and molecular interactions. Structure and function studies of biopolymers, such as proteins, are already well-established; thanks to that, we have a broad range of tools to characterize biological macromolecules that facilitate research outcomes. However, we must refine and adjust existing protocols to characterize abiotic systems. Binding between abiotic sequence-defined oligomers and ligands can be induced by rational design based on supramolecular chemistry background. Oligourethanes equipped with structural motifs such as phenyl rings and hydrogen bond donors/acceptors enable attractive interactions with a bisphenol A ligand. Regardless of the stereocenter(s) mutation pattern, all sequences interact with a BPA primarily via vdW rather than electrostatic interaction despite a strongly nonpolar environment which would enhance the latter. The predominance of nondirectional vdW forces over directional interactions such as hydrogen bonding results in complex behavior with a low level of specificity. Studied systems display a range of possible complex conformations interacting with the ligand with different strengths yet showing similar binding characteristics. Such nature of attraction and liability may render it a nonspecific receptor. Since the dispersive forces are not directional, they allow the binding of structurally similar compounds. On the other hand, the flexibility of the macromolecule may enhance that effect by adopting diverse conformations depending on the type of ligand. Matching the shape of the oligomer and the ligand is a key to achieve a reliable binding, allowing the highest number of interactions and supramolecular bonds to be formed. Amplification of polymer molar mass is expected to cause an augmentation in the frequency and strength of interactions between the polyurethane and the ligand, as longer chains will have an increased number of sites to form hydrogen bonding, π-π stacking, and Van der Waals interactions. We speculate that the elongation of polymers to the level of protein size will improve specificity of binding with the ligand. Moreover, to improve the design of oligourethanes we should consider the additional polar groups to forge an impactful number

and strength of directional electrostatic interactions between molecules. To advance the specificity of the convoluted binding mechanism of BPA a broad sequence space of oligomers must be explored to find matching structural motifs. The demonstrated MD simulation methodology is emerging as an invaluable tool for the in-silico screening of various structures to optimize receptor-like functionalities of oligourethanes. The method reveals the impact of subtle structural changes, such as the effect of stereocenter sequence (e.g., 1 kcal ΔG_{bind} difference). As we demonstrated for NMR and CD spectroscopies, such flexible systems are challenging to characterize by structure-sensitive methodologies. We considered fluorescence measurements a complementary technique for verifying simulation data. The observed fluorescence quenching is not too sensitive to the structural diversity of complexes and delivers data representative of the whole ensemble of conformations. Combining the developed MD methodology with the Stern-Volmer model is an efficient strategy for predicting and validating receptor-like functionalities of oligomer ligand complexes that can be used for future structure optimization and the development of sensory materials using abiotic sequences and sterocontrolled polymers.

Supporting Information

Supporting information contains all experimental details, spectra (NMR, CD, fluorescence), chromatograms (LC-MS, GPC), and a detailed description of simulations.

Author Contributions

R.S. conceived and designed the study, evaluated data, and supervised experimental work. T.A. designed and supervised theoretical studies. M.S. performed theoretical calculations, synthesis of oligourethanes, and characterization (NMR, GPC, LC-MS). W.F. and S.K. performed experimental work on synthesizing oligourethanes and ligand-oligomers interaction studies by

NMR, CD, and fluorescence. All authors helped to prepare the manuscript and analyzed and discussed the data. All authors have approved the final version of the manuscript.

Funding

Polish National Science Centre grant No. 2018/31/D/ST5/01365; National Centre for Research and Development project No. LIDER/27/0148/L-12/20/NCBR/2021; Łukasiewicz Centre grant No. 4/Ł-PORT/CŁ/2021

Conflicts of Interest

There are no conflicts to declare.

Acknowledgments

R.S., M.S. (NCN scholarship) are highly grateful to the Polish National Science Centre (2018/31/D/ST5/01365) for financial support. R.S. and S.K. thank the Łukasiewicz Centre for the financial support grant PolyProbe: 4/Ł-PORT/CŁ/2021. R.S. and W.F. thank the National Centre for Research and Development for funding the project (LIDER/27/0148/L-12/20/NCBR/2021). Calculations have been carried out using resources provided by the Wrocław Centre for Networking and Supercomputing (http://wcss.pl). We thank Janusz Skonieczny (NMR), Patrick Groves (NMR), and Katarzyna Kapczynska (LC-MS) for technical support during the analyses.

References

(1) Laurent, E.; Szweda, R.; Lutz, J. Synthetic Polymers with Finely Regulated Monomer Sequences: Properties and Emerging Applications. In *Macromolecular Engineering*; Wiley, 2022; pp 1–34. https://doi.org/10.1002/9783527815562.mme0041.

(2) Lutz, J.-F. Defining the Field of Sequence-Controlled Polymers. *Macromol Rapid Commun* **2017**, *38* (24), 1700582. https://doi.org/10.1002/MARC.201700582.

(3) Hawker, C. J.; Wooley, K. L. The Convergence of Synthetic Organic and Polymer Chemistries. *Science* **2005**, *309* (5738), 1200–1205. https://doi.org/10.1126/SCIENCE.1109778.

(4) Lutz, J.-F.; Ouchi, M.; Liu, D. R.; Sawamoto, M. Sequence-Controlled Polymers. *Science* **2013**, *341* (6146), 1238149. https://doi.org/10.1126/science.1238149.

(5) Aksakal, R.; Mertens, C.; Soete, M.; Badi, N.; Du Prez, F. Applications of Discrete Synthetic Macromolecules in Life and Materials Science: Recent and Future Trends. *Advanced Science* **2021**, *8* (6), 2004038. https://doi.org/10.1002/advs.202004038.

(6) Solleder, S. C.; Schneider, R. V.; Wetzel, K. S.; Boukis, A. C.; Meier, M. A. R. Recent Progress in the Design of Monodisperse, Sequence-Defined Macromolecules. *Macromol Rapid Commun* **2017**, *38* (9), 1600711. https://doi.org/10.1002/marc.201600711.

(7) DeStefano, A. J.; Segalman, R. A.; Davidson, E. C. Where Biology and Traditional Polymers Meet: The Potential of Associating Sequence-Defined Polymers for Materials Science. *JACS Au* **2021**, *1* (10), 1556–1571. https://doi.org/10.1021/jacsau.1c00297.

(8) Meier, M. A. R.; Barner-Kowollik, C. A New Class of Materials: Sequence-Defined Macromolecules and Their Emerging Applications. *Adv Mat* **2019**, *31* (26), 1806027. https://doi.org/10.1002/adma.201806027.

(9) RN Zuckermann, JM Kerr, SB Kent, W. M. Efficient Method for the Preparation of Peptoids [Oligo (N-Substituted Glycines)] by Submonomer Solid-Phase Synthesis. *J Am Chem Soc* **1992**, *114*, 10646–10647.

(10) Rosales, A. M.; Segalman, R. A.; Zuckermann, R. N. Polypeptoids: A Model System to Study the Effect of Monomer Sequence on Polymer Properties and Self-Assembly. *Soft Matter* **2013**, *9* (35), 8400–8414. https://doi.org/10.1039/C3SM51421H.

(11) A Al Ouahabi, L Charles, J.-F. L. Synthesis of Non-Natural Sequence-Encoded Polymers Using Phosphoramidite Chemistry. *J Am Chem Soc* **2015**, *137*, 5629–5635.

(12) Li, J.; Leclercq, M.; Fossepré, M.; Surin, M.; Glinel, K.; Jonas, A. M.; Fernandes, A. E. Discrete Multifunctional Sequence-Defined Oligomers with Controlled Chirality. *Polym Chem* **2020**, *11* (24), 4040–4046. https://doi.org/10.1039/d0py00537a.

(13) Charles, L.; Cavallo, G.; Monnier, V.; Oswald, L.; Szweda, R.; Lutz, J.-F. MS/MS-Assisted Design of Sequence-Controlled Synthetic Polymers for Improved Reading of Encoded Information. *J Am Soc Mass Spectrom* **2017**, *28* (6), 1149–1159. https://doi.org/10.1007/s13361-016-1543-5.

(14) Wang, X.; Zhang, X.; Ding, S. 1,2,3-Triazole-Based Sequence-Defined Oligomers and Polymers. *Polym Chem* **2021**, *12* (18), 2668–2688. https://doi.org/10.1039/D1PY00123J.

(15) Fischer, L.; Guichard, G. Folding and Self-Assembly of Aromatic and Aliphatic Urea Oligomers: Towards Connecting Structure and Function. *Org Biomol Chem* The Royal Society of Chemistry July 2010, pp 3102–3117. https://doi.org/10.1039/c001090a.

(16) Gunay, U. S.; Petit, B. E.; Karamessini, D.; Al Ouahabi, A.; Amalian, J.-A.; Chendo, C.; Bouquey, M.; Gigmes, D.; Charles, L.; Lutz, J.-F. Chemoselective Synthesis of Uniform Sequence-Coded Polyurethanes and Their Use as Molecular Tags. *Chem* **2016**, *1* (1), 114–126. https://doi.org/10.1016/j.chempr.2016.06.006.

(17) Martens, S.; Van den Begin, J.; Madder, A.; Du Prez, F. E.; Espeel, P. Automated Synthesis of Monodisperse Oligomers, Featuring Sequence Control and Tailored Functionalization. *J Am Chem Soc* **2016**, *138* (43), 14182–14185. https://doi.org/10.1021/jacs.6b07120.

(18) Forysiak, W.; Kozub, S.; John, Ł.; Szweda, R. Discrete Oligourethanes of Sequence-Regulated Properties – Impact of Stereocontrol. *Polym Chem* **2022**, *13* (20), 2980–2987. https://doi.org/10.1039/D2PY00299J.

(19) Dahlhauser, S. D.; Escamilla, P. R.; Vandewalle, A. N.; York, J. T.; Rapagnani, R. M.; Shei, J. S.; Glass, S. A.; Coronado, J. N.; Moor, S. R.; Saunders, D. P.; Anslyn, E. V. Sequencing of Sequence-Defined Oligourethanes via Controlled Self-Immolation. *J Am Chem Soc* **2020**, *142* (6), 2744–2749. https://doi.org/10.1021/JACS.9B12818/SUPPL_FILE/JA9B12818_SI_001.PDF.

(20) Zydziak, N.; Konrad, W.; Feist, F.; Afonin, S.; Weidner, S.; Barner-Kowollik, C. Coding and Decoding Libraries of Sequence-Defined Functional Copolymers Synthesized via Photoligation. *Nat Commun* **2016**, *7* (1), 1–13. https://doi.org/10.1038/ncomms13672.

(21) Dong, R.; Liu, R.; Gaffney, P. R. J.; Schaepertoens, M.; Marchetti, P.; Williams, C. M.; Chen, R.; Livingston, A. G. Sequence-Defined Multifunctional Polyethers via Liquid-Phase Synthesis with Molecular Sieving. *Nat Chem* **2019**, *11* (2), 136–145. https://doi.org/10.1038/s41557-018-0169-6.

(22) Lee, J. M.; Kwon, J.; Lee, S. J.; Jang, H.; Kim, D. G.; Song, J.; Kim, K. T. Semiautomated Synthesis of Sequence-Defined Polymers for Information Storage. *Sci Adv* **2022**, *8* (10), 8614. https://doi.org/10.1126/sciadv.abl8614.

(23) Takizawa, K.; Nulwala, H.; Hu, J.; Yoshinaga, K.; Hawker, C. J. Molecularly Defined (L)-Lactic Acid Oligomers and Polymers: Synthesis and Characterization. *J Polym Sci A Polym Chem* **2008**, *46* (18), 5977–5990. https://doi.org/10.1002/POLA.22944.

(24) Szweda, R.; Chendo, C.; Charles, L.; Baxter, P. N. W.; Lutz, J.-F. Synthesis of Oligoarylacetylenes with Defined Conjugated Sequences Using Tailor-Made Soluble Polymer Supports. *Chem Commun* **2017**, *53* (59), 8312–8315. https://doi.org/10.1039/C7CC03633G.

(25) Schneider, R. V.; Waibel, K. A.; Arndt, A. P.; Lang, M.; Seim, R.; Busko, D.; Bräse, S.; Lemmer, U.; Meier, M. A. R. Sequence-Definition in Stiff Conjugated Oligomers. *Sci Rep* **2018**, *8* (1), 17483. https://doi.org/10.1038/s41598-018-35933-z.

(26) Yu, H.; Li, S.; Schwieter, K. E.; Liu, Y.; Sun, B.; Moore, J. S.; Schroeder, C. M. Charge Transport in Sequence-Defined Conjugated Oligomers. *J Am Chem Soc* **2020**, *142* (10), 4852–4861. https://doi.org/10.1021/JACS.0C00043.

(27) Krywko-Cendrowska, A.; Szweda, D.; Szweda, R. Well-Defined Conjugated Macromolecules Based on Oligo(Arylene Ethynylene)s in Sensing. *Processes* **2020**, *8* (5), 539. https://doi.org/10.3390/PR8050539.

(28) He, W.; Wang, S.; Li, M.; Wang, X.; Tao, Y. Iterative Synthesis of Stereo- and Sequence-Defined Polymers via Acid-Orthogonal Deprotection Chemistry. *Angew Chem Int Ed* **2022**, *61* (9). https://doi.org/10.1002/anie.202112439.

(29) Ślęczkowski, M. L.; Segers, I.; Liu, Y.; Palmans, A. R. A. Sequence-Defined L-Glutamamide Oligomers with Pendant Supramolecular Motifs via Iterative Synthesis and Orthogonal Post-Functionalization. *Polym Chem* **2020**, *11* (46), 7393–7401. https://doi.org/10.1039/D0PY01157F.

(30) Mertens, C.; Soete, M.; Ślęczkowski, M. L.; Palmans, A. R. A.; Meijer, E. W.; Badi, N.; Du Prez, F. E. Stereocontrolled, Multi-Functional Sequence-Defined Oligomers through Automated Synthesis. *Polym Chem* **2020**, *11* (26), 4271–4280. https://doi.org/10.1039/D0PY00645A.

(31) Kwon, Y.; Kim, K. T. Crystallization-Driven Self-Assembly of Block Copolymers Having Monodisperse Poly(Lactic Acid)s with Defined Stereochemical Sequences. *Macromolecules* **2021**, *54* (22), 10487–10498. https://doi.org/10.1021/acs.macromol.1c01825.

(32) Szweda, R. Sequence- and Stereo-Defined Macromolecules: Properties and Emerging Functionalities. *Prog Polym Sci* **2023**, *145*, 101737. https://doi.org/10.1016/J.PROGPOLYMSCI.2023.101737.

(33) Leguizamon, S. C.; Scott, T. F. Mimicking DNA Functions with Abiotic, Sequence-Defined Polymers. *Polym Rev* **2022**, *62* (3), 626–651. https://doi.org/10.1080/15583724.2021.2014519.

(34) Rutten, M. G. T. A.; Vaandrager, F. W.; Elemans, J. A. A. W.; Nolte, R. J. M. Encoding Information into Polymers. *Nat Rev Chem* 2018, 365–381. https://doi.org/10.1038/s41570-018-0051-5.

(35) Lutz, J.-F. Coding Macromolecules: Inputting Information in Polymers Using Monomer-Based Alphabets. *Macromolecules* **2015**, *48* (14), 4759–4767. https://doi.org/10.1021/acs.macromol.5b00890.

(36) Mutlu, H.; Lutz, J. Reading Polymers: Sequencing of Natural and Synthetic Macromolecules. *Angew Chem Int Ed* **2014**, *53* (48), 13010–13019. https://doi.org/10.1002/anie.201406766.

(37) Roy, R. K.; Meszynska, A.; Laure, C.; Charles, L.; Verchin, C.; Lutz, J.-F. Design and Synthesis of Digitally Encoded Polymers That Can Be Decoded and Erased. *Nat Commun* **2015**, *6* (1), 7237. https://doi.org/10.1038/ncomms8237.

(38) Martens, S.; Landuyt, A.; Espeel, P.; Devreese, B.; Dawyndt, P.; Du Prez, F. Multifunctional Sequence-Defined Macromolecules for Chemical Data Storage. *Nat Commun* **2018**, *9* (1), 4451. https://doi.org/10.1038/s41467-018-06926-3.

(39) Boukis, A. C.; Reiter, K.; Frölich, M.; Hofheinz, D.; Meier, M. A. R. Multicomponent Reactions Provide Key Molecules for Secret Communication. *Nat Commun* **2018**, *9* (1), 1439. https://doi.org/10.1038/s41467-018-03784-x.

(40) Cao, C.; Krapp, L. F.; Ouahabi, A. Al; König, N. F.; Cirauqui, N.; Radenovic, A.; Lutz, J.-F.; Peraro, M. D. Aerolysin Nanopores Decode Digital Information Stored in Tailored Macromolecular Analytes. *Sci Adv* **2020**, *6* (50), eabc2661. https://doi.org/10.1126/SCIADV.ABC2661.

(41) König, N. F.; Al Ouahabi, A.; Oswald, L.; Szweda, R.; Charles, L.; Lutz, J.-F. Photo-Editable Macromolecular Information. *Nat Commun* **2019**, *10* (1), 3774. https://doi.org/10.1038/s41467-019-11566-2.

(42) Girvin, Z. C.; Andrews, M. K.; Liu, X.; Gellman, S. H. Foldamer-Templated Catalysis of Macrocycle Formation. *Science* **2019**, *366* (6472), 1528–1531. https://doi.org/10.1126/SCIENCE.AAX7344.

(43) Chandra, P.; Jonas, A. M.; Fernandes, A. E. Synthesis of Discrete Catalytic Oligomers and Their Potential in Silica-Supported Cooperative Catalysis. *RSC Adv* **2019**, *9* (25), 14194–14197. https://doi.org/10.1039/c9ra00847k.

(44) Celasun, S.; Maron, E.; Börner, H. G. Peptide-Assisted Design of Precision Polymer Sequences: On the Relevance of the Side-Chain Sequences and the Variability of the Backbone. *Macromol Biosci* **2020**, *20* (1), 1900244. https://doi.org/10.1002/mabi.201900244.

(45) Lawatscheck, C.; Pickhardt, M.; Wieczorek, S.; Grafmüller, A.; Mandelkow, E.; Börner, H. G. Generalizing the Concept of Specific Compound Formulation Additives towards Non-Fluorescent Drugs: A Solubilization Study on Potential Anti-Alzheimer-Active Small-Molecule Compounds. *Angew Chem Intl Ed* **2016**, *55* (30), 8752–8756. https://doi.org/10.1002/ANIE.201601147.

(46) Celasun, S.; Remmler, D.; Schwaar, T.; Weller, M. G.; Du Prez, F.; Börner, H. G. Digging into the Sequential Space of Thiolactone Precision Polymers: A Combinatorial Strategy to Identify Functional Domains. *Angew Chem Int Ed* **2019**, *58* (7), 1960–1964. https://doi.org/10.1002/ANIE.201810393.

(47) Patil, K. M.; Naik, R. J.; Rajpal; Fernandes, M.; Ganguli, M.; Kumar, V. A. Highly Efficient (R-X-R)-Type Carbamates as Molecular Transporters for Cellular Delivery. *J Am Chem Soc* **2012**, *134* (17), 7196–7199. https://doi.org/10.1021/ja210026m.

(48) Yadav, S.; Sharma, A. K.; Kumar, P. Nanoscale Self-Assembly for Therapeutic Delivery. *Front Bioeng Biotechnol* **2020**, *8*, 127. https://doi.org/10.3389/FBIOE.2020.00127/BIBTEX.

(49) Jose, A.; Nanjan, P.; Porel, M. Sequence-Defined Oligomer as a Modular Platform for Selective Sub-Picomolar Detection and Removal of Hg 2+. *Polym Chem* **2021**, *12* (36), 5201–5208. https://doi.org/10.1039/D1PY00642H.

(50) Jose, A.; Porel, M. Selective and Sensitive Fluorescent Staining of Serum Albumin in Protein Gel Electrophoresis via Sequence-Defined Oligo-Dithiocarbamate. *RSC Adv* **2023**, *13* (51), 35791–35798. https://doi.org/10.1039/D3RA06985K.

(51) Aksakal, R.; Tonneaux, C.; Uvyn, A.; Fosséprés, M.; Turgut, H.; Badi, N.; Surin, M.; De Geest, B. G.; Du Prez, F. E. Sequence-Defined Antibody-Recruiting Macromolecules. *Chem Sci* **2023**, *14* (24), 6572–6578. https://doi.org/10.1039/D3SC01507F.

(52) Boden, S.; Reise, F.; Kania, J.; Lindhorst, T. K.; Hartmann, L. Sequence-Defined Introduction of Hydrophobic Motifs and Effects in Lectin Binding of Precision Glycomacromolecules. *Macromol Biosci* **2019**, *19* (4), 1800425. https://doi.org/10.1002/mabi.201800425.

(53) Hartweg, M.; Jiang, Y.; Yilmaz, G.; Jarvis, C. M.; Nguyen, H. V.-T.; Primo, G. A.; Monaco, A.; Beyer, V. P.; Chen, K. K.; Mohapatra, S.; Axelrod, S.; Gómez-Bombarelli,

R.; Kiessling, L. L.; Becer, C. R.; Johnson, J. A. Synthetic Glycomacromolecules of Defined Valency, Absolute Configuration, and Topology Distinguish between Human Lectins. *JACS Au* **2021**, *1* (10), 1621–1630. https://doi.org/10.1021/JACSAU.1C00255.

(54) Wender, P. A.; Rothbard, J. B.; Jessop, T. C.; Kreider, E. L.; Wylie, B. L. Oligocarbamate Molecular Transporters: Design, Synthesis, and Biological Evaluation of a New Class of Transporters for Drug Delivery. *J Am Chem Soc* **2002**, *124* (45), 13382–13383. https://doi.org/10.1021/ja0275109.

(55) Nelli, Y. R.; Fischer, L.; Collie, G. W.; Kauffmann, B.; Guichard, G. Structural Characterization of Short Hybrid Urea/Carbamate (U/C) Foldamers: A Case of Partial Helix Unwinding. *Biopolymers* **2013**, *100* (6), 687–697. https://doi.org/10.1002/bip.22302.

(56) Wang, X.; Gan, Q.; Wicher, B.; Ferrand, Y.; Huc, I. Directional Threading and Sliding of a Dissymmetrical Foldamer Helix on Dissymmetrical Axles. *Angew Chem Int Ed* **2019**, *131* (13), 4249–4253. https://doi.org/10.1002/ange.201813125.

(57) Nguyen, H. V. T.; Jiang, Y.; Mohapatra, S.; Wang, W.; Barnes, J. C.; Oldenhuis, N. J.; Chen, K. K.; Axelrod, S.; Huang, Z.; Chen, Q.; Golder, M. R.; Young, K.; Suvlu, D.; Shen, Y.; Willard, A. P.; Hore, M. J. A.; Gómez-Bombarelli, R.; Johnson, J. A. Bottlebrush Polymers with Flexible Enantiomeric Side Chains Display Differential Biological Properties. *Nat Chem* **2022**, *14* (1), 85–93. https://doi.org/10.1038/s41557-021-00826-8.

(58) Becker, J.; Terracciano, R.; Yilmaz, G.; Napier, R.; Becer, C. R. Step-Growth Glycopolymers with a Defined Tacticity for Selective Carbohydrate-Lectin Recognition. *Biomacromolecules* **2023**, *24* (4), 1924–1933. https://doi.org/10.1021/acs.biomac.3c00133.

(59) Rezg, R.; El-Fazaa, S.; Gharbi, N.; Mornagui, B. Bisphenol A and Human Chronic Diseases: Current Evidences, Possible Mechanisms, and Future Perspectives. *Environ Int* **2014**, *64*, 83–90. https://doi.org/10.1016/j.envint.2013.12.007.

(60) Gies, A.; Soto, A. M. Bisphenol A: Contested Science, Divergent Safety Evaluations. *Late lessons from early warnings: science, precaution, innovation* **2013**, *II*, 215–239.

(61) Nizami, B.; Bereczki-Szakál, D.; Varró, N.; El Battioui, K.; Nagaraj, V. U.; Szigyártó, I. C.; Mándity, I.; Beke-Somfai, T. FoldamerDB: A Database of Peptidic Foldamers. *Nucleic Acids Res* **2020**, *48* (D1), D1122–D1128. https://doi.org/10.1093/nar/gkz993.

(62) Rinaldi, S. The Diverse World of Foldamers: Endless Possibilities of Self-Assembly. *Molecules* **2020**, *25* (14), 3276. https://doi.org/10.3390/molecules25143276.

(63) Martinek, T. A.; Fülöp, F. Peptidic Foldamers: Ramping up Diversity. *Chem Soc Rev* **2012**, *41* (2), 687–702. https://doi.org/10.1039/c1cs15097a.

(64) Perez Mellor, A. F.; Brazard, J.; Kozub, S.; Bürgi, T.; Szweda, R.; Adachi, T. B. M. Unveiling the Configurational Landscape of Carbamate: Paving the Way for Designing Functional Sequence-Defined Polymers. *J Phys Chem A* **2023**, *127* (35), 7309–7322. https://doi.org/10.1021/acs.jpca.3c02442.

(65) Qin, X.; Liu, M.; Yang, D.; Zhang, X. Concentration-Dependent Aggregation of CHAPS Investigated by NMR Spectroscopy. *J Phys Chem B* **2010**, *114* (11), 3863–3868. https://doi.org/10.1021/jp911720w.

(66) LaPlante, S. R.; Carson, R.; Gillard, J.; Aubry, N.; Coulombe, R.; Bordeleau, S.; Bonneau, P.; Little, M.; O'Meara, J.; Beaulieu, P. L. Compound Aggregation in Drug Discovery: Implementing a Practical NMR Assay for Medicinal Chemists. *J Med Chem* **2013**, *56* (12), 5142–5150. https://doi.org/10.1021/jm400535b.

(67) Tian, C.; Kasavajhala, K.; Belfon, K. A. A.; Raguette, L.; Huang, H.; Migues, A. N.; Bickel, J.; Wang, Y.; Pincay, J.; Wu, Q.; Simmerling, C. Ff19SB: Amino-Acid-Specific

Protein Backbone Parameters Trained against Quantum Mechanics Energy Surfaces in Solution. *J Chem Theory Comput* **2020**, *16* (1), 528–552. https://doi.org/10.1021/ACS.JCTC.9B00591/SUPPL_FILE/CT9B00591_SI_002.ZIP.

(68) Valdés-Tresanco, M. S.; Valdés-Tresanco, M. E.; Valiente, P. A.; Moreno, E. Gmx_MMPBSA: A New Tool to Perform End-State Free Energy Calculations with GROMACS. *J Chem Theory Comput* **2021**, *17* (10), 6281–6291. https://doi.org/10.1021/acs.jctc.1c00645.

(69) Schneider, P.; Willen, L.; Smulski, C. R. Tools and Techniques to Study Ligand–Receptor Interactions and Receptor Activation by TNF Superfamily Members. *Methods Enzymol* **2014**, *545*, 103–125. https://doi.org/10.1016/B978-0-12-801430-1.00005-6.

(70) Jing, M.; Bowser, M. T. Methods for Measuring Aptamer-Protein Equilibria: A Review. *Anal Chim Acta* **2011**, *686* (1–2), 9–18. https://doi.org/10.1016/J.ACA.2010.10.032.

(71) Ríos, P.; Mooibroek, T. J.; Carter, T. S.; Williams, C.; Wilson, M. R.; Crump, M. P.; Davis, A. P. Enantioselective Carbohydrate Recognition by Synthetic Lectins in Water. *Chem Sci* **2017**, *8* (5), 4056–4061. https://doi.org/10.1039/c6sc05399h.

(72) Zsila, F. Aromatic Side-Chain Cluster of Biotin Binding Site of Avidin Allows Circular Dichroism Spectroscopic Investigation of Its Ligand Binding Properties. *J Mol Recognit* **2011**, *24* (6), 995–1006. https://doi.org/10.1002/jmr.1147.

(73) Siligardi, G.; Hussain, R.; Patching, S. G.; Phillips-Jones, M. K. Ligand- and Drug-Binding Studies of Membrane Proteins Revealed through Circular Dichroism Spectroscopy. *Biochim Biophys Acta Biomembr* **2014**, *1838* (1 PARTA), 34–42. https://doi.org/10.1016/j.bbamem.2013.06.019.

(74) Bose, A. Interaction of Tea Polyphenols with Serum Albumins: A Fluorescence Spectroscopic Analysis. *J Lumin* **2016**, *169*, 220–226. https://doi.org/10.1016/j.jlumin.2015.09.018.

(75) Hwang, H.; Myong, S. Protein Induced Fluorescence Enhancement (PIFE) for Probing Protein-Nucleic Acid Interactions. *Chem Soc Rev* **2014**, *43* (4), 1221–1229. https://doi.org/10.1039/c3cs60201j.

(76) Zhao, Q.; Tao, J.; Feng, W.; Uppal, J. S.; Peng, H.; Le, X. C. Aptamer Binding Assays and Molecular Interaction Studies Using Fluorescence Anisotropy - A Review. *Anal Chim Acta* **2020**, *1125*, 267–278. https://doi.org/10.1016/j.aca.2020.05.061.

(77) Gáspári, Z.; Perczel, A. Protein Dynamics as Reported by NMR. In *Annual Reports on NMR Spectroscopy*; 2010; Vol. 71, pp 35–75. https://doi.org/10.1016/B978-0-08-089054-8.00002-2.

(78) VanScyoc, W. S.; Shea, M. A. Phenylalanine Fluorescence Studies of Calcium Binding to N-Domain Fragments of Paramecium Calmodulin Mutants Show Increased Calcium Affinity Correlates with Increased Disorder. *Protein Sci* **2001**, *10* (9), 1758–1768. https://doi.org/10.1110/ps.11601.

(79) Bose, A. Interaction of Tea Polyphenols with Serum Albumins: A Fluorescence Spectroscopic Analysis. *J Lumin* **2016**, *169*, 220–226. https://doi.org/10.1016/j.jlumin.2015.09.018.

(80) Hwang, H.; Myong, S. Protein Induced Fluorescence Enhancement (PIFE) for Probing Protein-Nucleic Acid Interactions. *Chem Soc Rev* **2014**, *43* (4), 1221–1229. https://doi.org/10.1039/c3cs60201j.

(81) Zhao, Q.; Tao, J.; Feng, W.; Uppal, J. S.; Peng, H.; Le, X. C. Aptamer Binding Assays and Molecular Interaction Studies Using Fluorescence Anisotropy - A Review. *Anal Chim Acta* **2020**, *1125*, 267–278. https://doi.org/10.1016/j.aca.2020.05.061.

(82) Dwarakanath, S.; Bruno, J. G.; Shastry, A.; Phillips, T.; John, A.; Kumar, A.; Stephenson, L. D. Quantum Dot-Antibody and Aptamer Conjugates Shift Fluorescence upon Binding

Bacteria. *Biochem Biophys Res Commun* **2004**, *325* (3), 739–743. https://doi.org/10.1016/j.bbrc.2004.10.099.

(83) Van De Weert, M. Fluorescence Quenching to Study Protein-Ligand Binding: Common Errors. *J Fluoresc* **2010**, *20* (2), 625–629. https://doi.org/10.1007/S10895-009-0572-X.

Table of Contents